Orbital Identification of Carbonate-Bearing Rocks on Mars

Bethany L. Ehlmann, *et al.*

Science **322**, 1828 (2008);
DOI: 10.1126/science.1164759

Large clutch volume–adult body mass ratios do not occur in dinosaurs more distantly related to birds, such as allosauroids (*26*). Troodontids and oviraptorids further differ from other more basal dinosaurs in featuring relatively larger eggs, monoautochronic ovulation, and brooding (*5*, *6*, *23*). Consequently, two factors may have contributed to the evolution of paternal care: (i) increased energy demands of larger, sequentially ovulated eggs, necessitating females to focus strictly on their own feeding and egg laying (*24*, *27*), and (ii) greater thermal incubation needs of embryos, requiring an attendant brooding adult (*28*). Because maternal and biparental care systems occur within extant crocodilians, the nature of parental care within more basal theropods and dinosaurs in general remains ambiguous.

Paternal care in both troodontids and oviraptorids (Fig. 2E) implies that this reproductive system originated before the origin of flight and was primitive for Aves. Biparental care of Neognathes would then represent a derived condition. Although paternal care has previously been suggested as the ancestral condition for extant birds (*3*, *24*, *27*, *29*), it has largely been envisioned as evolving within primitive birds, potentially in conjunction with superprecocial chicks (*24*, *27*). In extant birds, the three parental care strategies correspond to statistically distinct clutch volume–adult body mass relationships (table S2), with paternal care associated with the largest clutches, maternal care with intermediate-size clutches, and biparental care with the smallest clutches for most adult sizes. This suggests a trade-off in parental investment between overall clutch mass and total parental care.

References and Notes

1. T. H. Clutton-Brock, *The Evolution of Parental Care* (Princeton Univ. Press, Princeton, NJ, 1991).
2. B. S. Tullberg, M. Ah-King, H. Temrin, *Philos. Trans. R. Soc. London Ser. B* **357**, 251 (2002).
3. J. D. Ligon, *The Evolution of Avian Breeding Systems* (Oxford Univ. Press, Oxford, 1999).
4. S. J. J. F. Davies, *Ratites and Tinamous* (Oxford Univ. Press, Oxford, 2002).
5. D. J. Varricchio, F. Jackson, J. J. Borkowski, J. R. Horner, *Nature* **385**, 247 (1997).
6. M. A. Norell, J. M. Clark, L. M. Chiappe, D. Dashzeveg, *Nature* **378**, 774 (1995).
7. See supporting material on *Science* Online.
8. H. Motulsky, A. Christopoulos, *Fitting Models to Biological Data Using Linear and Nonlinear Regression* (Oxford Univ. Press, Oxford, 2004).
9. W. R. Branch, R. W. Patterson, *J. Herpetol.* **9**, 243 (1975).
10. L. H. S. Van Mierop, S. M. Barnard, *J. Herpetol.* **10**, 333 (1976).
11. O. Lourdais, T. C. M. Hoffman, D. F. DeNardo, *J. Comp. Physiol. B* **177**, 569 (2007).
12. L. A. Somma, *Smithsonian Herpetological Information Service 81* (1990).
13. R. Shine, in *Biology of the Reptilia*: *Volume 16, Ecology B*, C. Gans, R. B. Huey, Eds. (Liss, New York, 1988), pp. 276–329.
14. D. J. Varricchio, F. D. Jackson, *J. Vertebr. Paleontol.* **24**, 931 (2004).
15. C. S. Wink, R. M. Elsey, *J. Morphol.* **189**, 183 (1986).
16. K. Simkiss, *Calcium in Reproductive Physiology* (Chapman and Hall, London, 1967).
17. A. Chinsamy, *Palaeontol. Afr.* **27**, 77 (1990).
18. M. H. Schweitzer, J. L. Wittmeyer, J. R. Horner, *Science* **308**, 1456 (2005).
19. A. H. Lee, S. Werning, *Proc. Natl. Acad. Sci. U.S.A.* **105**, 582 (2008).
20. P. C. Sereno, *Science* **284**, 2137 (1999).
21. G. M. Erickson, K. C. Rogers, D. J. Varricchio, M. A. Norell, X. Xu, *Biol. Lett.* **3**, 558 (2007).
22. R. Pahl, D. W. Winkler, J. Graveland, B. W. Batterman, *Proc. R. Soc. London Ser. B* **264**, 239 (1997).
23. D. J. Varricchio, F. D. Jackson, in *Feathered Dragons*, P. J. Currie, E. B. Koppelhus, M. A. Shugar, J. L. Wright, Eds. (Indiana Univ. Press, Bloomington, 2004), pp. 215–233.
24. A. Elzanowksi, in *Acta XVIII Congressus Internationalis Ornithologici*, V. D. Ilyichev, V. M. Gavrilov, Eds. (Academy of Sciences of the USSR, Moscow, 1985), pp. 178–183.
25. J. R. Horner, in *Dinosaurs Past and Present, Volume II*, S. J. Czerkas, E. C. Olson, Eds. (Univ. of Washington Press, Seattle, 1987), pp. 51–63.
26. I. Mateus *et al.*, *C. R. Acad. Sci. Paris IIA* **325**, 71 (1997).
27. T. Wesolowski, *Am. Nat.* **143**, 39 (1994).
28. S. L. Vehrencamp, *Behav. Ecol.* **11**, 334 (1999).
29. J. Van Rhijn, *Neth. J. Zool.* **34**, 103 (1984).

30. We thank J. Horner, A. Chinsamy-Turan, L. Hall, H. Akashi, J. Rotella, and P. T. Varricchio Sr. Supported by NSF grants EAR-0418649 and DBI-0446224 (G.M.E.).

Supporting Online Material

www.sciencemag.org/cgi/content/full/322/5909/1826/DC1
Materials and Methods
Tables S1 to S5
References

14 July 2008; accepted 14 November 2008
10.1126/science.1163245

Orbital Identification of Carbonate-Bearing Rocks on Mars

Bethany L. Ehlmann,[1] John F. Mustard,[1] Scott L. Murchie,[2] Francois Poulet,[3] Janice L. Bishop,[4] Adrian J. Brown,[4] Wendy M. Calvin,[5] Roger N. Clark,[6] David J. Des Marais,[7] Ralph E. Milliken,[8] Leah H. Roach,[1] Ted L. Roush,[7] Gregg A. Swayze,[6] James J. Wray[9]

Geochemical models for Mars predict carbonate formation during aqueous alteration. Carbonate-bearing rocks had not previously been detected on Mars' surface, but Mars Reconnaissance Orbiter mapping reveals a regional rock layer with near-infrared spectral characteristics that are consistent with the presence of magnesium carbonate in the Nili Fossae region. The carbonate is closely associated with both phyllosilicate-bearing and olivine-rich rock units and probably formed during the Noachian or early Hesperian era from the alteration of olivine by either hydrothermal fluids or near-surface water. The presence of carbonate as well as accompanying clays suggests that waters were neutral to alkaline at the time of its formation and that acidic weathering, proposed to be characteristic of Hesperian Mars, did not destroy these carbonates and thus did not dominate all aqueous environments.

Although telescopic measurements hinted at the presence of carbonate on Mars (*1*–*3*), subsequent orbiting and landed instruments found no large-scale or massive carbonate-bearing rocks (*4*, *5*). Carbonate in veins within Martian meteorites (*6*) and possibly at <5% abundance in Mars dust (*1*, *4*) indicates that it is present as a minor phase. The lack of carbonate-bearing rock outcrops is puzzling in light of evidence for surface water and aqueous alteration, which produced sulfate and phyllosilicate minerals (*5*, *7*). Carbonate is an expected weathering product of water and basalt in an atmosphere with CO_2 (*8*, *9*), and large-scale deposits, which might serve as a reservoir for atmospheric CO_2, were predicted for Mars (*10*). Lack of carbonate among identified alteration minerals has compelled suggestions that either (i) a warmer, wetter early Mars was sustained by greenhouse gases other than CO_2 (*11*, *12*); (ii) liquid water on Mars' surface in contact with its CO_2 atmosphere was not present for long enough to form substantial carbonate (*13*) (thus implying that minerals such as phyllosilicates must have formed in the subsurface); or (iii) formation of carbonate deposits was inhibited or all such deposits were destroyed by acidic aqueous activity (*14*, *15*) or by decomposition (*16*). Here we report the detection of carbonate in a regional-scale rock unit by the Mars Reconnaissance Orbiter's (MRO's) Compact Reconnaissance Imaging Spectrometer for Mars (CRISM) and discuss the implications for the climate and habitability of early Mars.

In targeted mode, CRISM acquires hyperspectral images from 0.4 to 4.0 μm in 544 channels at a spatial resolution of 18 meters per pixel (*17*). In addition to diverse hydrated silicates (*18*), CRISM identified a distinct, mappable

[1]Department of Geological Sciences, Brown University, Providence, RI 02912, USA. [2]Johns Hopkins University/Applied Physics Laboratory, 11100 Johns Hopkins Road, Laurel, MD 20723, USA. [3]Institut d'Astrophysique Spatiale, Université Paris Sud 11, 91405 Orsay, France. [4]SETI Institute and NASA Ames Research Center, 515 North Whisman Road, Mountain View, CA 94043, USA. [5]Department of Geological Sciences and Engineering, University of Nevada, MS 172, 1664 North Virginia Street, Reno, NV 89557, USA. [6]U.S. Geological Survey, MS 964, Box 25046, Denver Federal Center, Denver, CO 80225, USA. [7]NASA Ames Research Center, Mountain View, CA 94043, USA. [8]Jet Propulsion Laboratory, California Institute of Technology, MS 183-301, 4800 Oak Grove Drive, Pasadena, CA 91109, USA. [9]Department of Astronomy, Cornell University, 610 Space Sciences Building, Ithaca, NY 14853, USA.

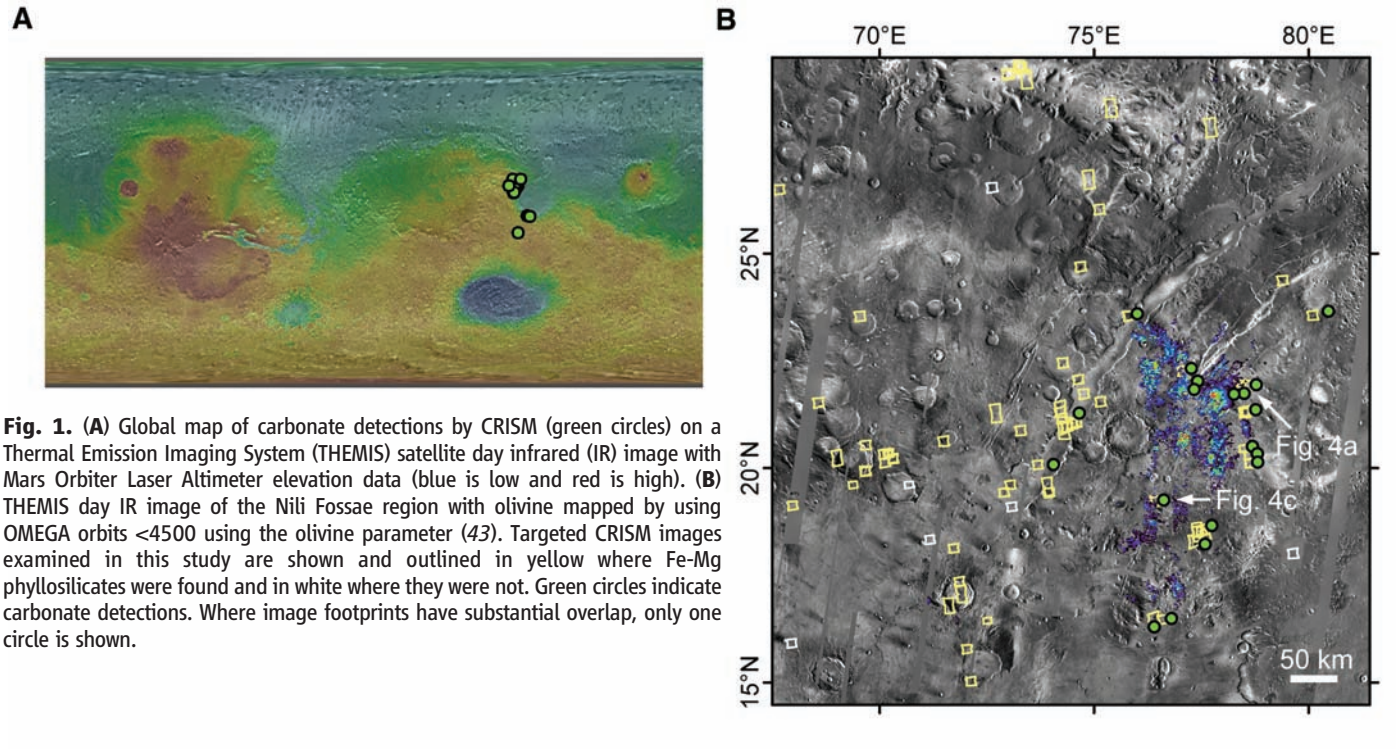

Fig. 1. (**A**) Global map of carbonate detections by CRISM (green circles) on a Thermal Emission Imaging System (THEMIS) satellite day infrared (IR) image with Mars Orbiter Laser Altimeter elevation data (blue is low and red is high). (**B**) THEMIS day IR image of the Nili Fossae region with olivine mapped by using OMEGA orbits <4500 using the olivine parameter (*43*). Targeted CRISM images examined in this study are shown and outlined in yellow where Fe-Mg phyllosilicates were found and in white where they were not. Green circles indicate carbonate detections. Where image footprints have substantial overlap, only one circle is shown.

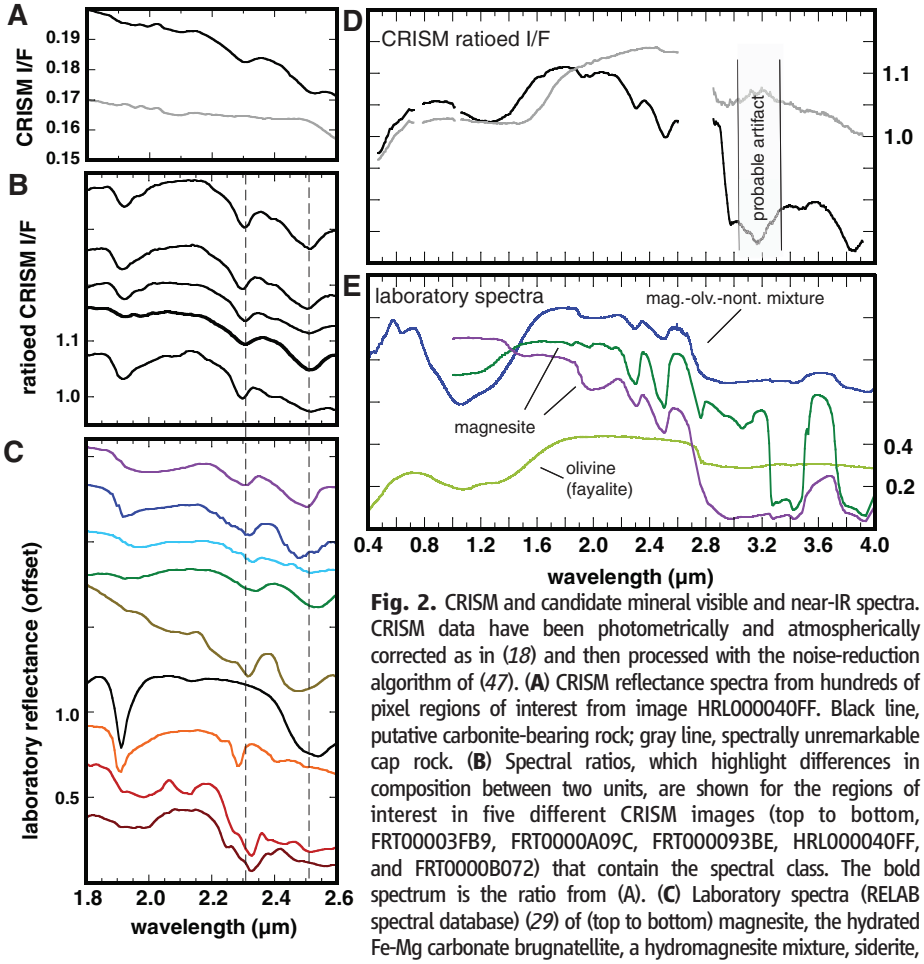

Fig. 2. CRISM and candidate mineral visible and near-IR spectra. CRISM data have been photometrically and atmospherically corrected as in (*18*) and then processed with the noise-reduction algorithm of (*47*). (**A**) CRISM reflectance spectra from hundreds of pixel regions of interest from image HRL000040FF. Black line, putative carbonite-bearing rock; gray line, spectrally unremarkable cap rock. (**B**) Spectral ratios, which highlight differences in composition between two units, are shown for the regions of interest in five different CRISM images (top to bottom, FRT00003FB9, FRT0000A09C, FRT000093BE, HRL000040FF, and FRT0000B072) that contain the spectral class. The bold spectrum is the ratio from (A). (**C**) Laboratory spectra (RELAB spectral database) (*29*) of (top to bottom) magnesite, the hydrated Fe-Mg carbonate brugnatellite, a hydromagnesite mixture, siderite, brucite, the zeolite analcime, nontronite, serpentine, and chlorite. (**D**) CRISM spectral ratios over the full wavelength range, using the same denominator, for terrains from HRL000040FF inferred to be carbonate-bearing (black) and olivine-bearing (gray). (**E**) Laboratory spectra for fayalitic olivine, magnesite, and a mixture of magnesite (80 wt %) and nontronite (5 wt %), sparsely covered with medium-grained olivine sand (15 wt %).

spectral class of hydrated material in the Nili Fossae region and two nearby areas (Fig. 1) for which a match to known mineral reflectance spectra was not initially evident (*19*). This spectral class has a 1.9-μm combination overtone from structural H_2O and also characteristic absorptions at 2.3 and 2.5 μm and a broad 1-μm absorption (Fig. 2). Similar spectra have been obtained with the Observatoire pour la Minéralogie, l'Eau, les Glaces, et l'Activité (OMEGA) imaging spectrometer on Mars Express (*20*).

Mg carbonate is the best candidate to explain the distinctive features of this spectral class. Paired absorptions at 2.3 and 2.5 μm are overtones and combination tones of C-O stretching and bending fundamental vibrations in the mid-infrared (*21*). The wavelength of their minima identifies the major metal cation in the carbonate (Fig. 3) (*21*, *22*). Anhydrous carbonates with mostly Mg exhibit minima at shorter wavelengths (2.30 and 2.50 μm) than those with mostly Ca (2.34 and 2.54 μm) and Fe (2.33 and 2.53 μm) (*22*) and match the spectral class identified by CRISM (Fig. 3). We know of no other mineral spectrum that has all of the properties of this class in terms of band position and width in the 2.0-to-2.6-μm spectral region (Fig. 2, B and C). The overall spectral shape, position, and relative strengths of the 2.3- and 2.5-μm absorption bands are consistent among CRISM spectra (Figs. 2B and 3), which suggests that the distinctive spectral class is generated by the presence of a single phase rather than a mixture of many alteration minerals (*23*). In a mixture, the relative strengths of individual bands would be expected to vary with variation in the relative abundances of the mineral

components. In some CRISM spectra of what we infer to be carbonate-bearing materials (Fig. 2B), intimate or spatial mixing is indicated by a wavelength shift and narrowing at 2.3 μm and broadening at 2.5 μm that is accompanied by the appearance of a weak band at 2.4 μm. These collectively indicate the presence also of iron-magnesium smectite [for example, nontronite (Fig. 2C, orange)], which has been previously identified in the region (*18*–*20*, *24*).

Although the distinctive CRISM spectroscopic signature was recognized in earlier OMEGA (*20*) and CRISM (*19*) observations, a carbonate mineral identification was rejected because the data lacked the strong 3.4- and 3.9-μm overtone absorptions seen in some laboratory data of calcite, other anhydrous carbonates (Fig. 2E, dark green), and their mixtures (*25*). However, we found the highly correlated 2.3- and 2.5-μm bands in many CRISM observations and thus reexamined the 3-to-4-μm region in both CRISM and laboratory data. Absorptions at 3.45 and 3.9 μm in the CRISM spectra are present in terrains with the 2.3/2.5-μm absorptions yet not in terrains lacking those absorptions [Fig. 2D and supporting online material (SOM) text] but are quite subtle and become apparent only after averaging of spectra from hundreds of pixels. Laboratory data show that absorptions from 3 to 4 μm in carbonate are not always strong (Fig. 2E, purple and blue). The presence of water, coatings, or additional minerals can reduce or eliminate these features. In the putative carbonate-bearing spectral class, the presence of a water-bearing phase (or phases) is indicated by 1.9-μm (Fig. 2B) and a deep 3.0-μm absorption (Fig. 2D). Hydrous carbonates (carbonates whose structures incorporate water) frequently have no 3.4- or 3.9-μm bands (*2*, *26*) and are a kinetically favored low-temperature alteration product from solutions with Mg and CO_3 (*9*, *27*, *28*). Strong overtones and fundamentals of water and OH near 3 μm in hydrated phases (for example, hydrous carbonates or clays) when mixed with anhydrous carbonate can subdue the 3-to-4-μm carbonate absorptions [Fig. 2E, blue; magnesite + hydromagnesite in (*21*, *29*)]. Additionally, remote detections in the 3-to-4-μm region are complicated by a thermal emission contribution that reduces band strength (*30*, *31*) and also by instrument effects. CRISM's signal-to-noise ratio is more than four times lower at wavelengths >2.7 μm, and interpretation of that region is additionally complicated by uncorrected out-of-order light (*17*) and a probable detector artifact at 3.18 μm. The combination of subtle absorption features at 3.4 and 3.9 μm and the distinctive 2.3- and 2.5-μm bands is consistent with the presence of carbonate.

The CRISM spectra also display a strong broad band near 1.1 μm, which is generated by electronic transitions of Fe^{2+} (*32*). Magnesite ($MgCO_3$) and siderite ($FeCO_3$) form a complete solid solution, and a strong broad electronic band centered near 1.1 μm is apparent with even <1 weight percent (wt %) iron without changing the position of the 2.3- and 2.5-μm bands (*21*) (Fig. 2E, dark green). Alternatively, the strong 1.1-μm band in the putative CRISM carbonate spectra might result from small amounts of olivine, which is commonly associated with the carbonate as discussed below. Indeed, a laboratory mixture of magnesite (80 wt %), olivine (15 wt %), and the Fe-rich smectite nontronite (5 wt %) produces a spectrum similar to that observed by CRISM (Fig. 2E, blue).

Thousands of CRISM-targeted images sampling Mars' surface have been examined for this phase (*33*). One image in Terra Tyrrhena and two in Libya Montes contain small exposures of carbonate-bearing rocks, but the largest and most clearly defined exposures are in the Nili Fossae region, found to date in 24 CRISM-targeted images (Fig. 1). The Mg carbonate is present in relatively bright rock units exposed over <10 km^2, which allows detection by OMEGA and CRISM but probably precludes definitive detection by the Thermal Emission Spectrometer (TES) with its larger spatial footprint. The carbonate-bearing materials are restricted to Noachian cratered terrain (*34*), and their brightness in nighttime thermal infrared images and morphology in High-Resolution Imaging Science Experiment (HiRISE) images indicates that they occur in lithified deposits. The carbonate is observed in eroded mesa topography around the fossae, rocks exposed on the sides of valleys in the Jezero crater watershed and elsewhere, and sedimentary rocks within Jezero crater (*35*).

The carbonate-bearing rocks are relatively bright-toned and are commonly fractured (Fig. 4). Like the regional smectite and olivine deposits in Nili Fossae (*18*, *36*, *37*), the carbonate-bearing rocks consistently lie stratigraphically beneath an unaltered mafic cap unit (Fig. 4). All CRISM images examined that exhibit carbonate also exhibit Fe-Mg smectite-bearing rock units. In many examples, the carbonate-bearing unit is clearly above the smectite-bearing unit (Fig. 4), although in some cases the relationship is indeterminate and lateral variations between smectite and carbonate create pixels that display mixtures of the phases. In places where both carbonates and aluminum phyllosilicates can be mapped clearly, the carbonate-bearing unit is always stratigraphically lower. The carbonate-bearing unit appears to occupy the same stratigraphic position as other nearby olivine-bearing units (*18*), namely beneath the mafic cap unit but above Fe-Mg smectite-bearing units.

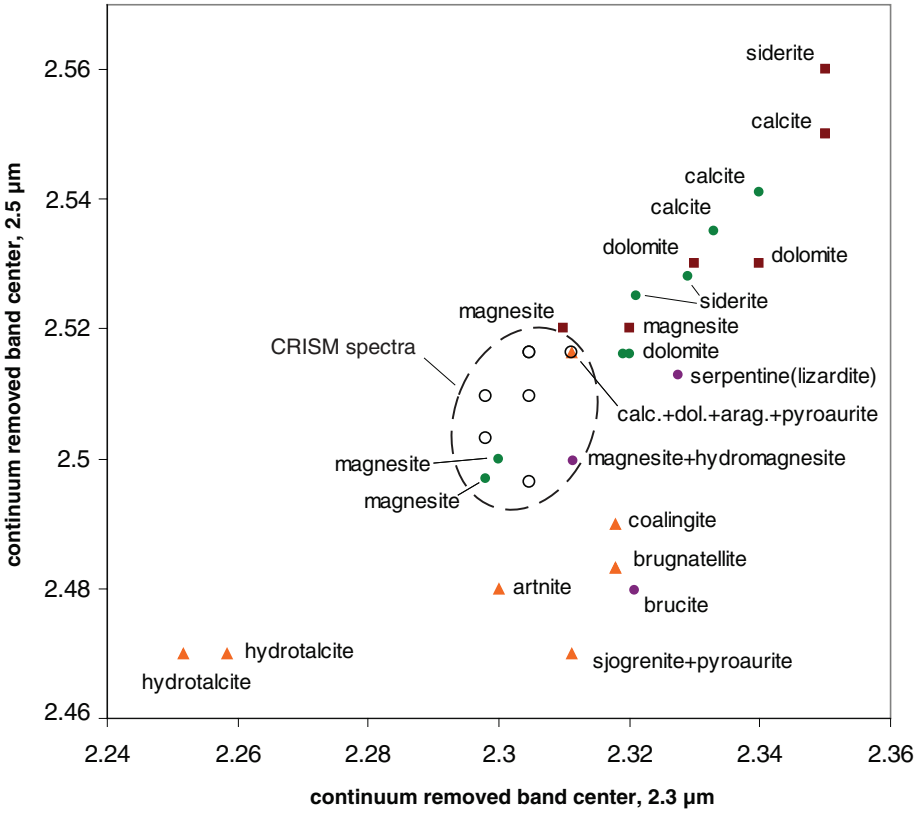

Fig. 3. Scatter plot of continuum-removed absorption band positions for anhydrous carbonates, hydrous carbonates, and other minerals with 2.3- and 2.5-μm absorptions. CRISM data that we identify as magnesite are shown as open circles within the larger dashed circle. Laboratory mineral spectra are shown from Gaffey (green circles) (*22*), Hunt and Salisbury (red squares) (*21*), RELAB spectra measured by E. Cloutis (orange triangles) (RELAB spectral database), and the USGS spectral library (purple circles) (*29*). Band centers of CRISM spectra are known to ±0.01 μm.

Whereas Fe-Mg smectites are found in a broad region extending westward to the Antoniadi basin (*19*), carbonate is restricted to the eastern portion of Nili Fossae (Fig. 1). This area is the most olivine-rich region so far observed on Mars (*38*, *39*) and has numerous valleys and sapping channels, which indicate that extensive surface fluvial activity extended into the early Hesperian (*36*).

We propose two possible formation settings to explain the origin, stratigraphy, and distribution of these carbonate-bearing rocks. First, the carbonate could have formed in the subsurface by groundwater percolating through fractures in the ultramafic rock and altering olivine. This may have occurred at only slightly elevated temperatures, as determined by the geothermal gradient. Alternatively, hot olivine-rich rocks excavated from deep in the crust by the Isidis impact (*37*) or volcanic flows (*39*, *40*) may have been deposited on top of water-bearing phyllosilicate rocks of the Noachian crust and may have initiated local hydrothermal alteration in a zone along the contact. The magnesite thus might occur in veined structures throughout olivine-rich rock, a relationship also observed in some Martian meteorites (*6*). These ultramafic rocks might have been serpentinized; however, CRISM has not yet conclusively identified serpentine.

An alternative explanation is that exposed olivine-rich rocks were weathered at surface ambient temperatures, perhaps during the surface fluvial activity in Nili Fossae that continued after the Isidis impact into the early Hesperian (*36*). The transformation of olivine-rich rocks to magnesite under cold dry conditions on Mars might resemble the weathering of olivine-rich meteorites in Antarctica (*41*), which produces magnesite and iron oxide mineral assemblages as rock rinds and/or coatings. A more water-rich surface-formation scenario would be that carbonate precipitated in shallow ephemeral lakes (*42*) from waters enriched in Mg^{2+} relative to other cations by percolation through ultramafic olivine-bearing rocks. Either scenario implies that surface conditions in the Nili Fossae region were sufficiently wet to cause chemical weathering during the late Noachian or early Hesperian eras.

The Nili Fossae carbonates do not appear to have sequestered large quantities of CO_2. With the possible exception of carbonate in transported sedimentary units within Jezero crater (*35*), we found no evidence of classic bedded sedimentary carbonate rocks resembling those on Earth. Instead, our results are consistent with carbonates having formed in response to specific local conditions. Although olivine is globally distributed on Mars (*43*, *44*), ultramafic rocks and their substantial interaction with water may have been necessary to generate carbonate in sufficient quantities to be detected from orbit at resolutions of tens of meters per pixel. Mg-carbonate–bearing rocks found at Nili Fossae, and perhaps also carbonate present at scales undetectable by CRISM, may contribute to a few percent magnesite in dust indicated by TES (*4*).

The existence of carbonate in rocks on Mars implies that neutral-to-alkaline waters existed at the time of their formation. Such conditions are consistent with those indicated by Fe-Mg smectite formation during the Noachian (*5*, *11*, *24*) but contrast with the acid, low-water-activity conditions thought to prevail over at least some of Mars during later time periods (*5*, *45*). The survival of the Nili Fossae carbonates indicates that they escaped destruction by exposure to acidic conditions, which would have dissolved the carbonate. Because aqueous activity in the Nili Fossae region extended into the Hesperian era (*36*), these carbonate-bearing rock units indicate that not all aqueous crustal environments experienced the acidic sulfate-forming conditions proposed to be characteristic of the planet during the Hesperian era, approximately 3.5 billion years ago (*5*, *46*). Ancient Mars apparently hosted aqueous environments in a variety of geologic settings in which waters ranged from the acidic to the alkaline. Such diversity bodes well for the prospect of past habitable environments on Mars.

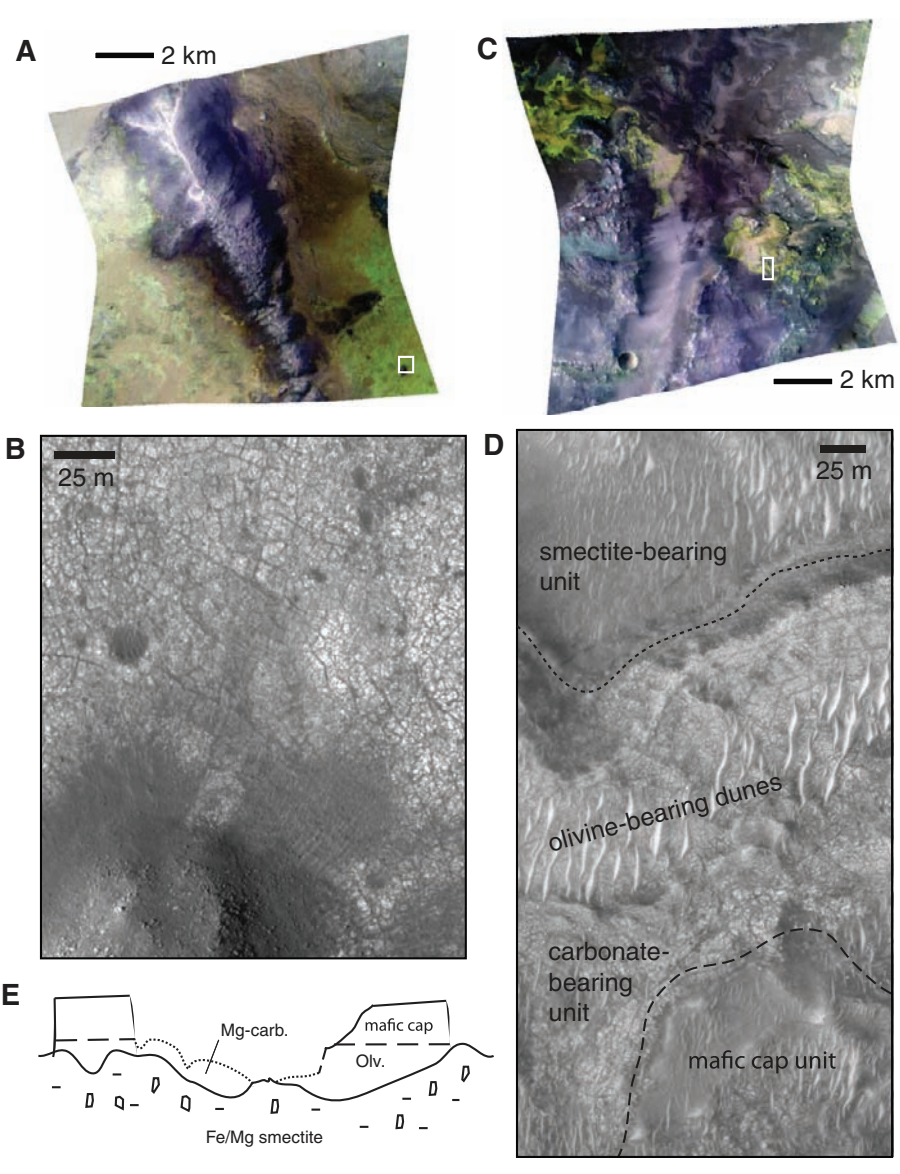

Fig. 4. Geomorphology and stratigraphy of the carbonate-bearing units. (**A**) CRISM false-color composite of FRT0000B072 (R, 2.38 μm; G, 1.80 μm; and B, 1.15 μm) where carbonate is green, olivine is yellow to brown, phyllosilicate is blue, and the mafic cap unit is purple. (**B**) subset of HiRISE PSP_002532_2020 from the white box in (A) showing a mafic knob overlying carbonate-bearing terrain. (**C**) FRT000093BE with colors as in (A). (**D**) Subset of HiRISE PSP_006778_1995 from the white box in (C), which shows the stratigraphy of carbonate-bearing units. (**E**) Schematic stratigraphy of the mineralogic units in the Nili Fossae region (not to scale).

References and Notes

1. J. B. Pollack *et al.*, *J. Geophys. Res.* **95**, 14595 (1990).
2. W. M. Calvin *et al.*, *J. Geophys. Res.* **99**, 14659 (1994).
3. E. Lellouch *et al.*, *Planet. Space Sci.* **48**, 1393 (2000).
4. J. L. Bandfield *et al.*, *Science* **301**, 1084 (2003).
5. J.-P. Bibring *et al.*, *Science* **312**, 400 (2006).
6. J. C. Bridges *et al.*, *Space Sci. Rev.* **96**, 365 (2001).

7. S. W. Squyres *et al.*, *Science* **306**, 1698 (2004).
8. J. L. Gooding, *Icarus* **33**, 483 (1978).
9. D. C. Catling, *J. Geophys. Res.* **104**, 16453 (1999).
10. J. B. Pollack *et al.*, *Icarus* **71**, 203 (1987).
11. V. Chevrier *et al.*, *Nature* **448**, 60 (2007).
12. I. Halevy *et al.*, *Science* **318**, 1903 (2007).
13. P. R. Christensen, in *Sixth International Conference on Mars* (Lunar and Planetary Institute, Houston, TX, 2003), abstract 3126.
14. A. G. Fairen *et al.*, *Nature* **431**, 423 (2004).
15. M. A. Bullock, J. M. Moore, *Geophys. Res. Lett.* **34**, L19201 (2007).
16. L. M. Mukhin, *Nature* **379**, 141 (1996).
17. S. Murchie *et al.*, *J. Geophys. Res.* **112**, E05S03 (2007).
18. J. F. Mustard *et al.*, *Nature* **454**, 305 (2008).
19. B. L. Ehlmann *et al.*, in *Seventh International Conference on Mars* (Lunar and Planetary Institute, Houston, TX, 2007), abstract 3270.
20. F. Poulet *et al.*, in *Seventh International Conference on Mars* (Lunar and Planetary Institute, Houston, TX, 2007), abstract 3170.
21. G. R. Hunt, J. W. Salisbury, *Mod. Geol.* **2**, 23 (1971).
22. S. J. Gaffey, *J. Geophys. Res.* **92**, 1429 (1987).
23. A multicomponent mineral assemblage of approximately constant proportions (for example, brucite + analcime + Fe-Mg smectite + olivine) is a possible alternative explanation for the observed position of the 2.3- and 2.5-μm features and their relative strengths. However, alteration assemblages are typically compositionally variable. Especially over the 10^5 km^2 considered here and in light of the 3.4- and 3.9-μm bands, a fixed-proportion multicomponent mixture is less plausible geologically than a contribution from a single component, namely Mg carbonate.
24. F. Poulet *et al.*, *Nature* **438**, 623 (2005).
25. D. Jouglet *et al.*, in *Seventh International Conference on Mars*, (Lunar and Planetary Institute, Houston, TX, 2007), abstract 3153.
26. E. A. Cloutis *et al., Lunar Planet Sci. Conf.* **31**, abstract 1152 (2000).
27. M. Hanchen *et al.*, *Chem. Eng. Sci.* **63**, 1012 (2008).
28. E. Konigsberger *et al.*, *Geochim. Cosmochim. Acta* **63**, 3105 (1999).
29. R. N. Clark *et al.*, U.S. Geological Survey (USGS) Digital Spectral Library splib06a, USGS Digital Data Series 231 (USGS, Denver, CO, 2007).
30. C. Wagner, U. Schade, *Icarus* **123**, 256 (1996).
31. D. Blaney, T. McCord, *J. Geophys. Res.* **94**, 10,159 (1989).
32. R. G. Burns, *Mineralogical Applications of Crystal Field Theory* (Cambridge Univ. Press, ed. 2, Cambridge, 1993).
33. Thousands of targeted CRISM images acquired through January 2008 in dust-free terrains were searched by coauthors and team members for this spectral class in the course of ongoing investigations. Additionally, all regions with OMEGA codetections of both olivine and hydration or phyllosilicate were investigated by the coauthors where CRISM images were available. Large Nili Fossae–scale regional carbonate units are unlikely to have been missed. Small outcrops of carbonate-bearing rock may yet be found elsewhere as more high-resolution CRISM data are acquired.
34. R. Greeley, J. E. Guest, "Geological Map of the Eastern Equatorial Region of Mars," *U.S. Geol. Surv. Misc. Inv. Series Map I-1802-B* (1987).
35. B. L. Ehlmann *et al.*, *Nat. Geosci.* **1**, 355 (2008).
36. N. Mangold *et al.*, *J. Geophys. Res.* **112**, E08S04 (2007).
37. J. F. Mustard *et al.*, *J. Geophys. Res.* **112**, E08S03 (2007).
38. T. M. Hoefen *et al.*, *Science* **302**, 627 (2003).
39. V. E. Hamilton, P. R. Christensen, *Geology* **33**, 433 (2005).
40. L. Tornabene *et al., J. Geophys. Res.*, 10.1029/2007JE002988 (2008).
41. A. J. T. Jull *et al.*, *Science* **242**, 417 (1988).
42. V. A. Melezhik *et al.*, *Sedimentology* **48**, 379 (2001).
43. F. Poulet *et al.*, *J. Geophys. Res.* **112**, E08S02 (2007).
44. W. C. Koeppen, V. E. Hamilton, *J. Geophys. Res.* **113**, E05001 (2008).
45. N. J. Tosca *et al.*, *Science* **320**, 1204 (2008).
46. J. A. Hurowitz, S. M. McLennan, *Earth Planet. Sci. Lett.* **260**, 432 (2007).
47. M. Parente, *Lunar and Planet Sci. Conf.* **39**, abstract 2528 (2008).

48. We thank R. Arvidson, R. Morris, N. Mangold, A. Baldridge, J.-P. Bibring, D. Jouglet, A. Fraeman, S. Wiseman, A. McEwen, G. Marzo, P. McGuire, and M. Wyatt for thoughtful discussions during manuscript preparation and E. Cloutis and others who have made quality spectral libraries available and contributed to the building of the NASA/Keck Reflectance Experiment Laboratory (RELAB) spectral database. We are grateful for the ongoing efforts of the MRO science and engineering teams, in particular the CRISM team, which enable these discoveries.

Supporting Online Material

www.sciencemag.org/cgi/content/full/322/5909/1828/DC1
SOM Text
Figs. S1 and S2
Table S1
References

18 August 2008; accepted 3 November 2008
10.1126/science.1164759

The Circadian Clock in *Arabidopsis* Roots Is a Simplified Slave Version of the Clock in Shoots

Allan B. James,[1] José A. Monreal,[1] Gillian A. Nimmo,[1] Ciarán L. Kelly,[1] Pawel Herzyk,[2,3] Gareth I. Jenkins,[1] Hugh G. Nimmo[1]*

The circadian oscillator in eukaryotes consists of several interlocking feedback loops through which the expression of clock genes is controlled. It is generally assumed that all plant cells contain essentially identical and cell-autonomous multiloop clocks. Here, we show that the circadian clock in the roots of mature *Arabidopsis* plants differs markedly from that in the shoots and that the root clock is synchronized by a photosynthesis-related signal from the shoot. Two of the feedback loops of the plant circadian clock are disengaged in roots, because two key clock components, the transcription factors CCA1 and LHY, are able to inhibit gene expression in shoots but not in roots. Thus, the plant clock is organ-specific but not organ-autonomous.

Many organisms have circadian clocks that temporally regulate their physiology and behavior and contribute to fitness (*1*–*3*). The eukaryotic clock involves gene expression feedback loops, with both negative and positive elements, and cytosolic signaling molecules (*4*–*7*). In the model plant *Arabidopsis*, the clock mechanism is thought to include at least three interlocking feedback loops (*5*, *8*, *9*). The central loop comprises two partially redundant MYB domain transcription factors, CIRCADIAN CLOCK ASSOCIATED1 (CCA1) and LATE ELONGATED HYPOCOTYL (LHY), which inhibit expression of a pseudo-response regulator TIMING OF CAB EXPRESSION1 (TOC1) (also known as PSEUDO-RESPONSE REGULATOR1, PRR1), whereas TOC1 activates expression of *CCA1* and *LHY* by an unknown mechanism (*5*, *10*–*12*). In the morning-phased loop, CCA1 and LHY activate the expression of *PSEUDO-RESPONSE REGULATOR7* (*PRR7*) and *PSEUDO-RESPONSE REGULATOR9* (*PRR9*) (*13*, *14*); the evening-phased loop involves TOC1 and GIGANTEA (GI) (see legend to fig. S12 for further information). These conclusions are based on experiments using whole seedlings grown in the presence of sucrose, without consideration of organ specificity. Yet, one major function of the plant clock involves the temporal partitioning of metabolic pathways via the control of output gene expression (*15*), and metabolism is inherently organ-specific. We therefore analyzed the circadian clock separately in shoots and roots of mature, hydroponically grown *Arabidopsis* plants (*16*).

Following transfer of plants from 12 hours light/12 hours dark (LD) to constant light (LL), *LHY* and *CCA1* transcripts continued to oscillate in both shoots and roots for three full cycles, with some damping (Fig. 1A and fig. S1), as determined by quantitative real-time reverse transcription polymerase chain reaction (qPCR). Notably, the period was some 2 hours longer in roots than in shoots; analysis of LHY protein (fig. S2) gave a similar result. *PRR9* and *PRR7* transcripts oscillated in both organs, with the time of peak expression later in roots than in shoots (fig. S3). *TOC1* transcripts in shoots oscillated in LL, in antiphase to those of *CCA1* and *LHY*, as expected. In marked contrast, *TOC1* transcripts in roots dipped slightly during the first subjective day in LL, then remained at a high level without oscillations (Fig. 1B and table S1). In shoots, oscillations in TOC1 protein were detectable for at least two cycles, whereas in roots TOC1 was present, with little variation, for 72

[1]Division of Molecular and Cellular Biology, Faculty of Biomedical and Life Sciences, University of Glasgow, Glasgow G12 8QQ, UK. [2]Division of Integrated Biology, Faculty of Biomedical and Life Sciences, University of Glasgow, Glasgow G12 8QQ, UK. [3]The Sir Henry Wellcome Functional Genomics Facility, Faculty of Biomedical and Life Sciences, University of Glasgow, Glasgow G12 8QQ, UK.

*To whom correspondence should be addressed. E-mail: h.g.nimmo@bio.gla.ac.uk